Chapter 3

Dielectric Resonator Nantennas for Optical Communication

Waleed Tariq Sethi, Hamsakutty Vettikalladi,
Habib Fathallah and Mohamed Himdi

Additional information is available at the end of the chapter

http://dx.doi.org/10.5772/intechopen.69064

Abstract

Dielectric resonator antennas (DRA) are ceramic based materials that are nonmetallic in nature. They offer high permitivity values (ε_r: 10-100). DRAs' have made their mark in various applications specially in the microwave and millimeter wave (MMW) spectrum, and are making encouraging progress in the THz band, because of their low conduction losses and higher radiation efficiencies compared to their metallic counterparts. With the advancements in nano fabrication, metallic antennas designed in the THz band have taken an interest. These antennas are termed as optical antennas or nantennas. Optical antennas work by receiving the incident electromagnetic wave or light and focusing it on a certain point or hot spot. Since most of the antennas are metallic based with Noble metals as radiators, the conducting losses are huge. One solution that we offer in this work is to integrate the nantennas with DRs. Two different DR based designs, one triangular and other hexagonal, are presented. Both the antennas operate in the optical C-band window (1550 nm). We design, perform numerical analysis, simulate, and optimize the proposed DR nantennas. We also consider array synthesis of the proposed nantennas in evaluating how much directive the nantennas are for use in nano network applications.

Keywords: dielectric resonator (DR), optical nanoantenna, hexagonal DR nantenna, triangular nantenna, optical communication C-window

1. Introduction

Over the last few years, with the introduction of various portable and wireless handheld devices, a surge in mobile and internet data traffic has been observed. This drastic increase is also effected

by the way our society creates, shares and consumes information on a regular basis. These abundant data and information sharing also demand for increase in delivery time. High data rate communication with compact size of device is the new norm in technology. Researchers and industry are working at a fast pace to fulfil their consumers demands. It is estimated that wireless data rates are getting doubled every year and are quickly approaching the provided capacity of the wired communication systems [1–5]. Following this trend, systems working at higher data rates are needed. Although millimetre waves and 60 GHz radio [6–9] currently provide a solution and are being implemented in 5G applications, still researchers have to think ahead of time. The electromagnetic spectrum has a lot of bands to offer in terms of wide bandwidth. One section of the spectrum that has not been explored completely in the Terahertz (THz) band can offer communication in the Terabit-per-second (Tbps) domain. These (Tbps) links can be realised over the next 10 years. Terahertz band communication [10–14] is intended as a key wireless technology to satisfy this growing demand of bandwidth-hungry devices with requirements of higher data rates. Since THz band is in the early exploring phase, a lot of revisions and new standards have to be designed for the systems operating at these higher bands of the electromagnetic spectrum (ultraviolet band-infrared band). Special considerations have to be made in the design of transmission and receiving portion of the THz system [15].

Antenna is an important component of any wireless system. For the antenna to be designed at this higher end of the spectrum (THz band), special tools are needed from its realisation to characterisation. The antennas designed at this spectrum are termed as optical nanoantennas [16]. Optical nanoantennas work on the operating principle that the electromagnetic (EM) wave or the light wave received can be controlled or placed into localised energy spots pertaining to the design of the nanoantenna. This property of the optical nanoantennas have gained immense interest from the research point of view as it can be applied to various fields of applications, such as spectroscopy, sensing, photodetection, metasurfaces, medicine, photovoltaics and energy-harvesting applications[17–20]. With the advancements in nanotechnology fabrication, the nanoantennas designed at THz band can be realised. Nanotechnology is a fast-growing research area that marked use of machines that can fabricate nanocomponents. It is considered as an enabling technology for a set of applications in biomedical, environmental and military fields as shown in **Figure 1**. Being inherently simple and performing primitive operations only, nanomachines in isolation are not expected to manage advanced tasks. To enable more complex applications such as intra-body drug delivery or cooperative environment sensing, the exchange of information and commands between networking entities and/or external controller is required. The need for coordination and information sharing naturally leads towards the concept of nanonetworks. One promising way to enable networking capabilities is to use wireless communications between nanomachines [21] made possible with optical nanoantennas fabricated on these machines.

Optical nanoantennas present some similarities with their radio frequency (RF) counterparts, yet there still exists some major difference. The main challenge arises from the fabrication tolerances at nanoscales and from the drastic deviation of metals from perfect conductors to lossy plasmonic materials at optical frequencies [22]. This is usually described as the well-known dispersive plasmonic effects and results in a significant decrease of radiation efficiency caused by conduction losses. These losses can be theoretically explained via different models at

http://dx.doi.org/10.5772/intechopen.69064

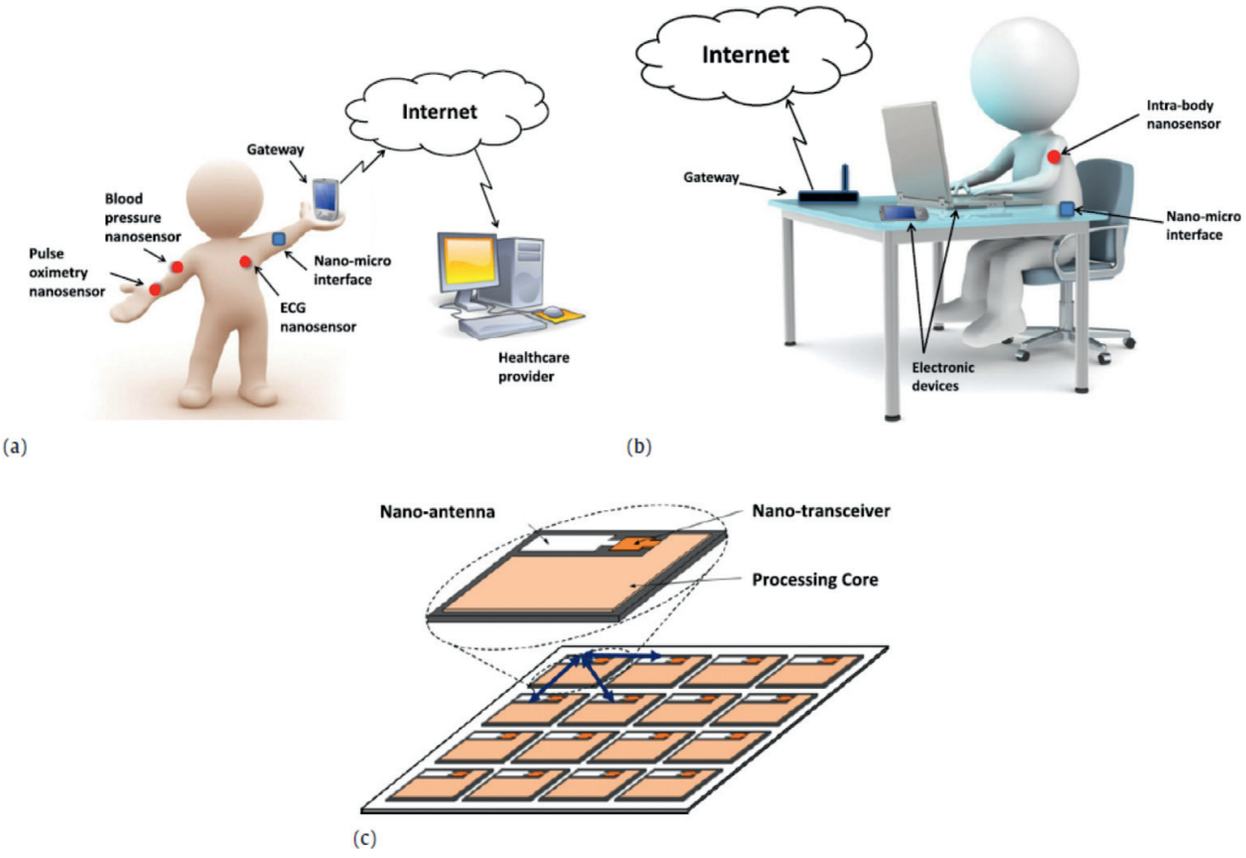

Figure 1. Applications for terahertz band (nanoscale antennas) [15].

specific frequencies with mostly known models such as Drude and Lorrentz model [23, 24]. One solution that is proposed in this chapter to cope with these metallic losses at high frequencies and to fully utilise the properties of metallic nanostructures is to design resonators or absorbers made with dielectric-based materials such as ceramics.

The idea of using antennas based on dielectric resonators (DR) was first proposed by Long et al. in 1983 [25], and since then the research into this novel idea is steadily increasing among the antenna researchers. The operation of DRAs as radiators exploit the 'radiation losses' of dielectric resonators made of moderate to high relative permittivity ($5 < \varepsilon_r < 100$) when excited in their lower order resonant modes in an open environment. Over the years, various aspects of DR antennas have been published and designs patented [26, 27]. Most notable publications are seen at the antennas operating as filters and circuits integrators at the microwave regime due to their compact size and high resistibility to losses. One striking feature of DR resonators is that they are immune to ohmic losses, which drastically appear at higher frequencies (bands above millimetre waves till far infrared), making them suitable candidates for optical nanoantennas. DRs are very efficient radiators compared to metallic antennas even at higher frequencies [28]. In this context, the work presented in this chapter focuses on integrating the resilient DR with metallic nanoelements for operating at THz band. The losses incurred due to appearing of

plasmonics inside the metal elements are subsided with the integration of various DR-shaped resonating elements. The results presented in the later sections validate the selection of DR as a suitable candidate and replacement to traditional metallic resonators working at higher THz band.

2. State-of-the-art antennas

Optical nanoantennas are an attractive area for research in the field of optics and nanophotonics. With the advent of nanofabrication machines, the antennas designed at the lower RF and microwave millimetre wave (MMW) domains can now be scaled up to the THz domain. Thus, some of the properties and analysis obtained for antenna designs at the lower band can be applied to higher bands. To study the effects and analyse the current distributions on the optical nanoantennas, a new branch of physics emerged known as nanophotonics. Nanophotonics studies the transmission and reception of optical signals by submicron and even nanometre-sized objects. For nanooptics, it is important to efficiently detect and direct the transmitting signals for optical information between nanoelements. The sources and detectors of radiation in nanooptics are nanoelements themselves, their clusters and even individual molecules (atoms, ions). Nano objects functioning as antennas must exhibit high radiation efficiency and directivity [29, 30]. Most of the nanoantennas existing in the literature are based on plasmonic metallic structures (**Figure 2**). In Ref. [31], dipole nanoantennas exhibit the electric field localisation at certain spots, whereas the bowtie nanoantennas presented in Ref. [32] present broadband characteristics; and in Ref. [33], Yagi-Uda displays high directive nature which can be useful for nanonetwork communication among nanoscaled devices. Similarly in Refs. [34, 35], plasmonic nanoantennas provide enhanced and controllable light-matter interactions and strong coupling between far-field radiation and localised sources at the nanoscale. In Refs. [36, 37], magneto-plasmonic response of the nanoantennas is observed when ferromagnetic metals are driven not only by light but also by external magnetic fields. The authors observed that the magneto-plasmonic nanoantennas enhance the magneto-optical effects, which introduces additional degrees of freedom in the control of light at the nanoscale. However, regardless of various advantages of plasmonic nanoantennas associated with their small size and strong localisation of the electric field, such nanoantennas have large dissipative losses resulting in low radiation efficiency.

To alleviate this conduction loss phenomenon, we propose a combination of DR and plasmonic metallic-based optical nanoantennas. Literature review shows some of the existing designs that perform well when working with DRs. Since DR offers high dielectric constant and refractive index values of the materials, the losses are minimised and subsided when integrated or placed with metallic resonators. In rest of the sections, we detail the proposed DR-based nanoantenna designs with simulated results. The enhancement in the directivity of the nanoantenna is also discussed by implementing an array structure of 1×2 ETDRNA elements. Also, the tunability of the nanoantenna array is discussed. Finally, the chapter ends with the conclusion section discussing the presented results based on selected DR design geometries.

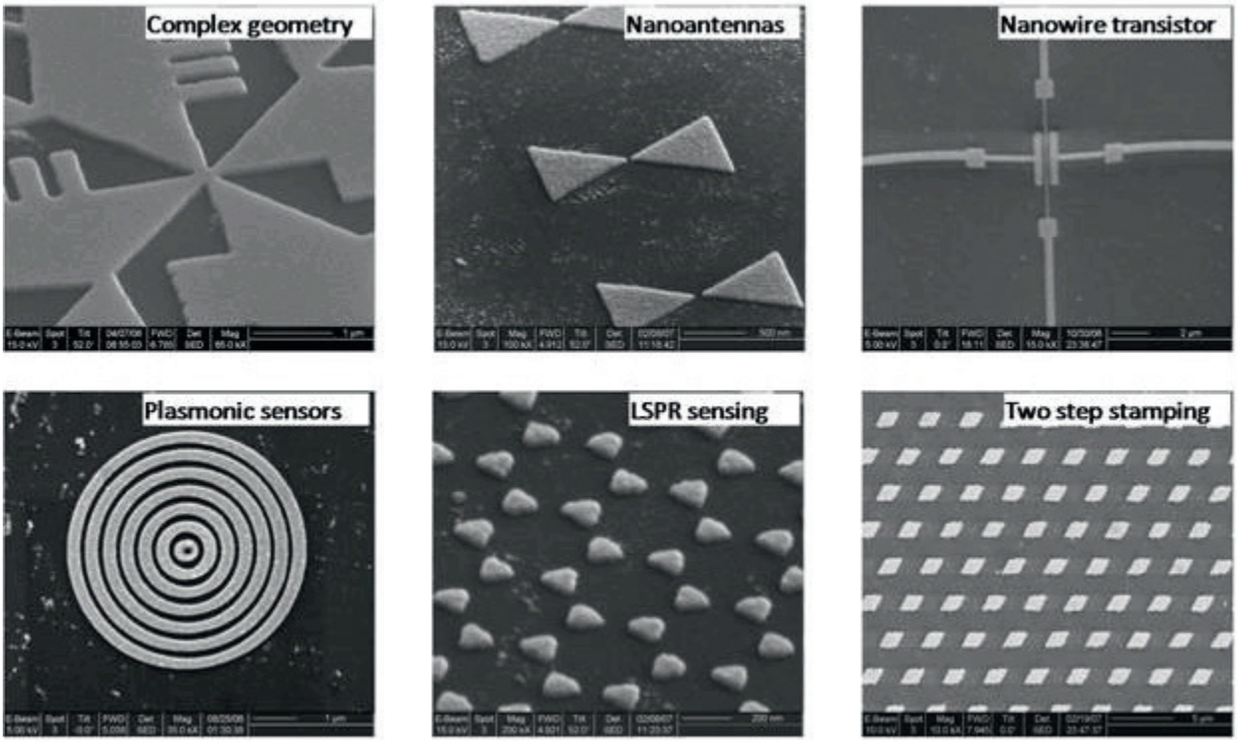

Figure 2. Different types of plasmonic nanoantennas: (a) complex connection, (b) bowtie, (c) dipole nanowires, (d) spiral sensor, (e) bowtie sensors and (f) rectangular patches [38].

Although we know that realization of any device is the ultimate proof of its operation, but at these very high THz frequencies it is difficult to have them fabricated as per limitations in fabrication resources. Secondly, our proposed designs are very small in dimensions (as will be discussed in later sections) to be realized currently with the exiting nano fabrication tools. Therefore we present the simulated designs using two different DR based resonators that we think will be viable candidates for designers and researchers who are in need of antenna designs having minimum losses and better radiation characteristics in the optical communication C-band at 1550 nm.

3. Equilateral triangular dielectric resonator nantenna

In this section, we present the simulated design and analysis of an equilateral triangular dielectric resonator nantenna (ETDRNA). The proposed nantenna is composed of a multilayer 'Ag-SiO_2-Ag' structure with noble metal silver (Ag) working as a feed transmission line. The dielectric triangular is made of silicon (Si) material and is excited via coupling mechanism from the feed line. The antenna yields a wide impedance bandwidth of 2.58% (192.3–197.3 THz) with a high directive radiation pattern of 8.6 dBi at 193.5 THz (1550 nm) with an end-fire radiation pattern.

3.1. Antenna geometry

Figure 3 shows the configuration (cross-sectional and front view) of the proposed equilateral triangular dielectric resonator nantenna (ETDRNA). The nanoantenna is designed to operate as a receiving antenna that can capture energy from the free space. The operating band of interest lies in the standard optical communication band at a wavelength of 1550 nm, which corresponds to central frequency of 193.5 THz. From the geometric configuration presented in **Figure 3**, the design follows a basic multilayer substrate approach. A silicon substrate (Si) having an oxide layer (O_2) is sandwiched between two conducting materials layers. The SiO_2 substrate has properties of thickness of h_1 = 0.150 μm, ε_r = 2.09 and loss tangent $tan\ \delta$ = 0 [39]. The partial conducting material below the substrate acts as a ground plane. Its dimensions and

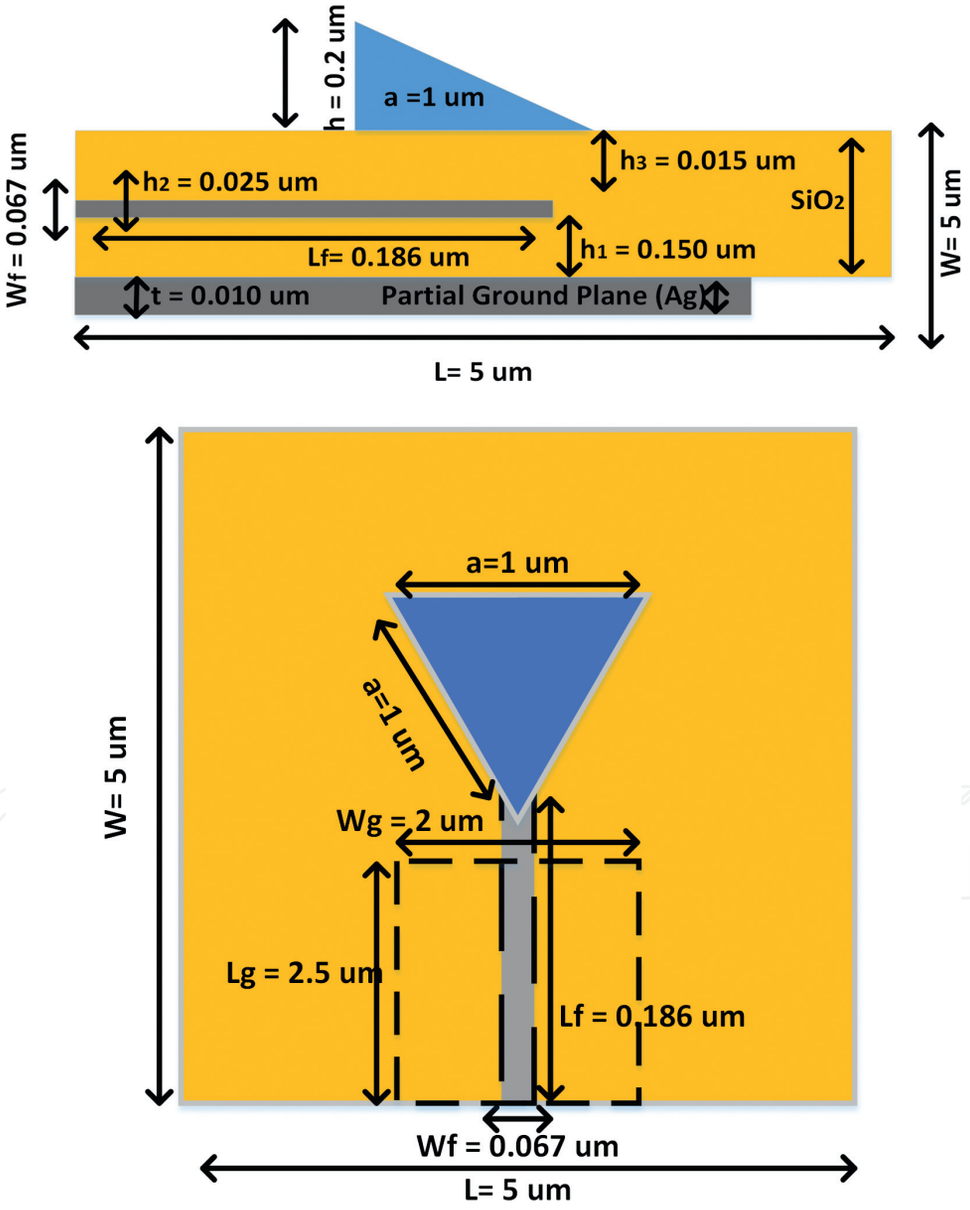

Figure 3. Antenna geometry of proposed nantenna design based on equilateral triangular DR (ETDRNA): (a) cross-sectional view; (b) front view.

thickness are $W_g \times L_g$ having a thickness of $t = 0.010$ μm. The nanoantenna is fed via a feed line placed on the top side of the substrate. It has geometric dimensions and thickness of $W_f \times L_f$; $h_2 = 0.025$ μm. The ground and the nanostrip are made up of noble metal silver (Ag). The dimensions of the substrate are taken as $W \times L = 5 \times 5$ μm^2. The resonator, made from (Si), placed on top of the feed line is made from dielectric material. It has the shape of an equilateral triangle with properties as $\varepsilon_r = 11.9$ and estimated loss tangent $tan\ \delta = 0.003$ at 100 THz [40]. The nanoantenna is excited and matched considering 50 Ω impedance source. In order to control the matching at the central frequency of 193.5 THz and to achieve a wide bandwidth with acceptable radiation patterns, the same (SiO_2) substrate material with thickness $h_3 = 0.015$ μm has been introduced between the equilateral triangle and the nanostrip. The dimensions of the equilateral triangular dielectric are calculated from Eq. (1) [41, 42].

$$f_{mnl} = \frac{c}{2\sqrt{\varepsilon_r}} \left[\sqrt{\left(\frac{4}{3a}\right)^2 + \left(\frac{p}{h}\right)^2} \right]^{1/2} \tag{1}$$

where 'a' is the side length of the equilateral triangular DRA, ε_r is the dielectric constant of the DRA, 'h' is two times the height of the triangular DRA to account for the image effect of the ground plane and $p = 1$ for the fundamental mode [42]. For a low-profile triangular DRA, we have $a >> h$, and therefore Eq. (2) demonstrates that the frequency is predominantly determined by the height of the DRA:

$$fr = \frac{c}{4h\sqrt{\varepsilon_r}} \tag{2}$$

where h and ε_r are the height and dielectric constant of triangular DRA.

Metals working in the optical regime are faced with another loss. This loss appears as negative permittivity, therefore complex permittivity ε_{Ag} of the metals, in our case silver (Ag), is calculated from Eq. (3) explained by the Drude model which is based upon kinetic theory of electron gas in solids [39]:

$$\varepsilon_{Ag} = \varepsilon_o \left\{ \varepsilon_\infty - \frac{f_{p^2}}{[f(f + i\gamma)]} \right\} = -129.17 + j3.28. \tag{3}$$

where $\varepsilon_o = 8.85 \times 10^{-12}$ [F/m], $\varepsilon_\infty = 5$, plasmonic frequency $f_p = 1.41e^{16}$ rad/s, f = central frequency and collision frequency $\gamma = 2.98e^{13}$. The plasmonic frequency, which appears after the photon and free electron gas collision, defines the collective motion of the electrons and can be expressed as follows:

$$f_p = \sqrt{ne^2/\varepsilon_0 m} \tag{4}$$

where n is electron concentration, e is the free electron charge (1.6×10^{-19} C), ε_0 is the free space (vacuum) permittivity (8.854×10^{-12} F/m) and m is the electron effective mass. From

Eq. (4), the behaviour of arriving EM wave to the metal can be deduced. For $f < f_p$ corresponds to and exponential decay field, EM wave will be reflected back and will not propagate through the metal. On the other hand, if $f > f_p$, the EM wave will behave as a travelling wave and will pass through the metals. Similarly, the collision or damping factor describes the losses within the metal and can be expressed as:

$$\gamma = \frac{e}{\mu m} \tag{5}$$

where μ is mobility of free carriers. The proposed model has taken into account the conductive and dielectric losses and has been simulated in commercially available EM simulator CST MWS 2014 based on FIT numerical technique using optical template.

3.2. Design simulation and optimisation

To get an understanding on the working principle of the proposed ETDRNA, various parameters of the nanoantenna were extensively optimised. In order to study the effects of the antenna performance in terms of bandwidth and directivity, the following parameters were observed and analysed.

a. **Nanostrip feed:** The nanostrip feed line placed on top of the SiO_2 substrate was optimised in terms of its length and width. The traditional empirical formulas [43] were used as a starting point for the nanostrip design. The nanostrip acts like a coupling resonator that excites the triangular dielectric place on an upper SiO_2 substrate with height h_3.Traditionally at RF frequencies, the length of the transmission lines are characterised to the wavelengths (λ) of incoming and outgoing radiations. However, working at the optical frequencies, the incident waves reflect less and penetrate more in to the substrate passing through the metal atoms. This phenomenon is known as plasmonic affect, and it gives rise to free plasmonic gaseous atoms. To deal with this new phenomenon at optical frequencies, we use shorter effective wavelength (λ_{eff}) compared to traditional wavelengths (λ), which depends on material characteristics given by Eq. (6) for length of a transmission line [44]:

$$\frac{m\lambda_{eff}}{2} = L(\lambda_o) \tag{6}$$

where Eq. (6) shows the relationship between the free space wavelength (λ_o) and the effective wavelength (λ_{eff}) and the order of resonance (m). Here, effective wavelength is given by:

$$\lambda_{eff} = \frac{\lambda_o}{n_{eff}} \tag{7}$$

Typical values of n_{eff} has been measured to be in the range of 1.5–3 [45]. In our case for the silver nanostrip feed line, we use $n_{eff} = 2.8$ which resulted the minimum resonating length of to be 0.27 μm. The length L_f of the nanostrip was optimised from 0.1 to 0.27 μm with the best optimised value producing required resonance at 193.5 THz was at $L_f = 0.186$ μm as shown in **Figure 4a**. The effect of the width *'W_f'* of the nanostrip was also examined by

extensive parametric studies. Initial values were taken from the empirical formulas [43] and optimisation was done from 0.02 to 0.28 μm. **Figure 4b** shows the best optimised value achieved at resonance of −22 dB with $W_f = 0.067$ μm.

b. **Partial ground plane:** The ground plane plays an important role in controlling the bandwidth and radiation characteristics of any designed antenna. At the nanoscale geometry, we simulated and observed its parameters effect on our nanoantennas resonance behaviour. We started off initially with a finite ground plane that achieved a good radiation pattern with an acceptable bandwidth. The ground plane was then optimised and a partial section of it was used with optimised dimensions $L_g \times W_g$ = 0.5 μm × 2 μm. **Figure 5a** and **b** shows the effects of varying the ground plane in terms of its length and width. The optimised results produce a wide impedance bandwidth of 2.5% (192.3–197.3 THz) at a centre frequency of 193.5 THz. This makes our proposed nanoantenna covers all the standard optical transmission widow (C-band), with a directivity of 8.6 dB.

c. **Height of triangular DR:** Since the height of the triangular DR predominately determines the resonance frequency as according to Eq. (2), the height h of the DR was optimised from 0.1 to 0.5 μm. **Figure 6** shows the best optimised value of h = 0.3 μm having a resonance at −23 dB.

d. **Rotation of triangular DR:** In order to study the effects of bandwidth, frequency shift and directivity of the nanoantenna design, the proposed silicon-based triangular DR was rotated on its axis. The rotation was from 0° to 360° with an angular spacing of 40°. **Figure 7** shows the angular rotation of the triangular DR. The tip of the triangle was initially aligned at 0° shown in green colour. The DR was then rotated along the counter-clockwise direction with varying angles. It was observed that with the rotation of the DR, the bandwidth remained the same at 2.5% but the resonant frequency shifted to other bands (200–205 THz) in the frequency range from (180–220 THz) as shown in **Figure 8a**. Since the triangle is an equilateral one, the angular rotation produces the same shifts at

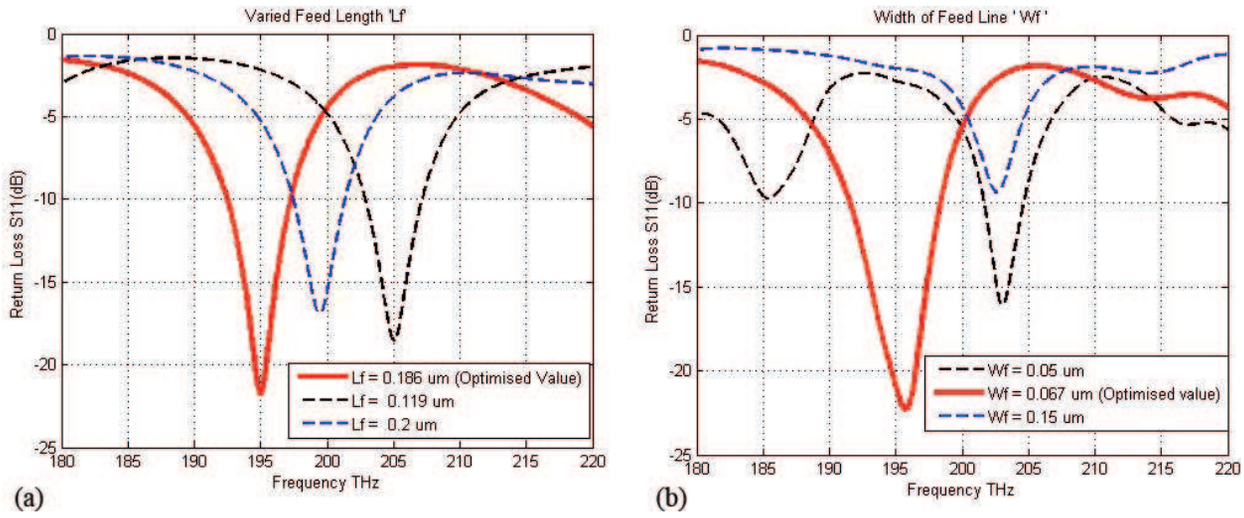

Figure 4. Optimized parameters: (a) length of feed line; (b) width of feed line.

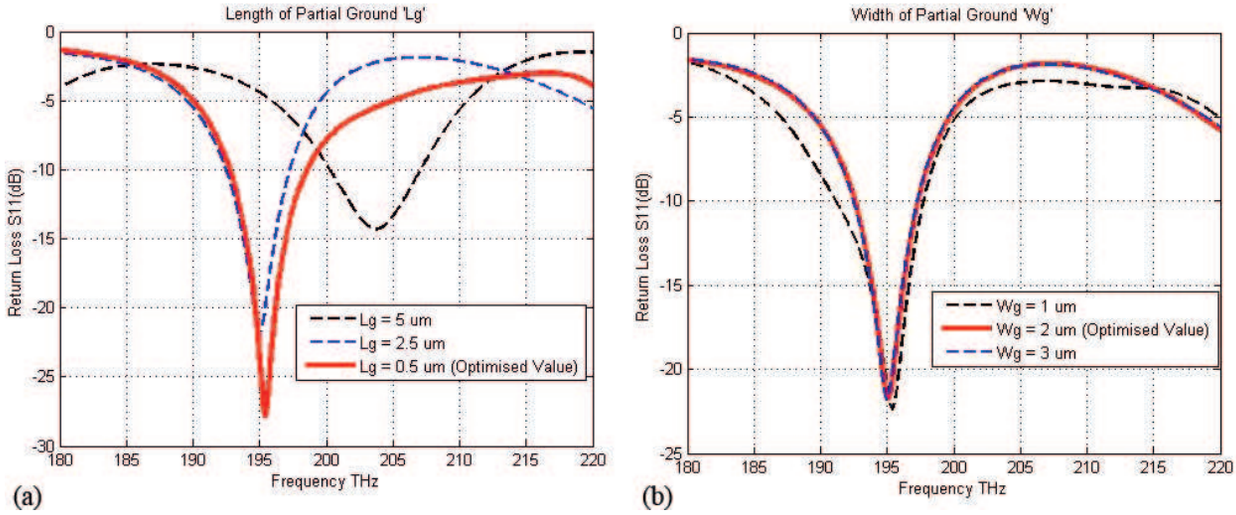

Figure 5. Optimized parameters: (a) length of ground plane; (b) width of ground plane.

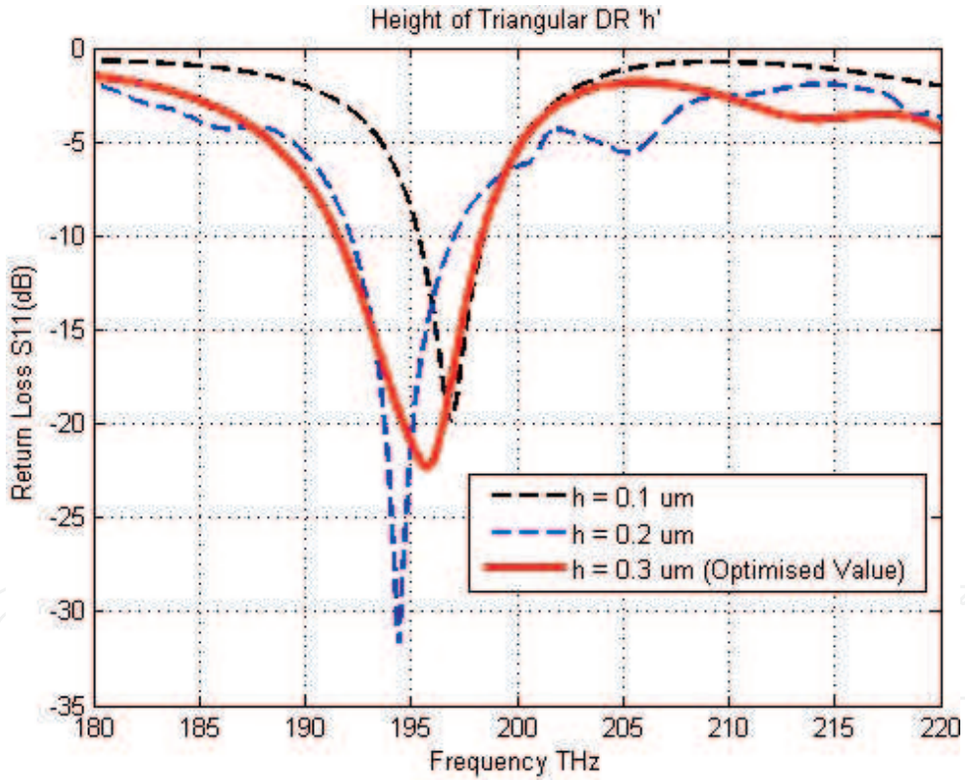

Figure 6. Optimized parameters: height of triangular DR.

other angles, that is, the shift will be the same at (0 = 120 = 240 = 360°) as shown in **Figure 8b**. The directivity was also affected with the rotation of the triangle as shown in **Figure 8b**. It is clear that the effect of the rotation of the triangular DR lowers the directivity to nearly 3 dBi.

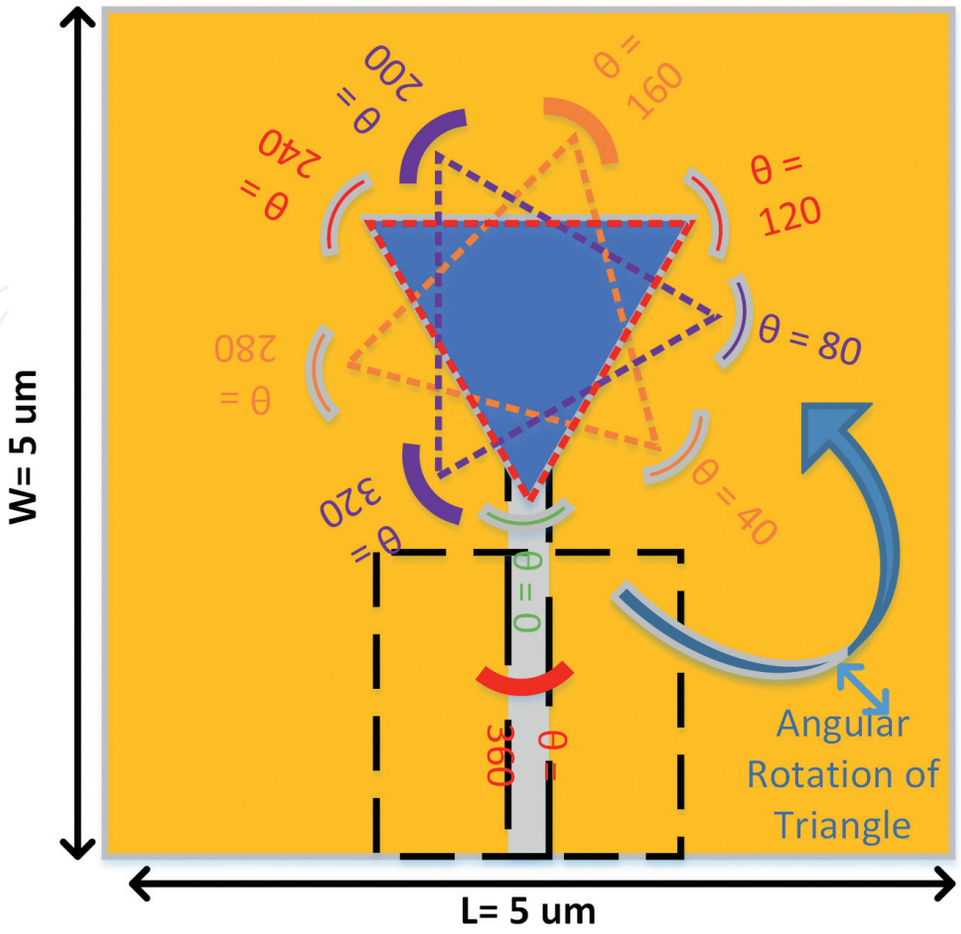

Figure 7. Angular rotation of triangular DR.

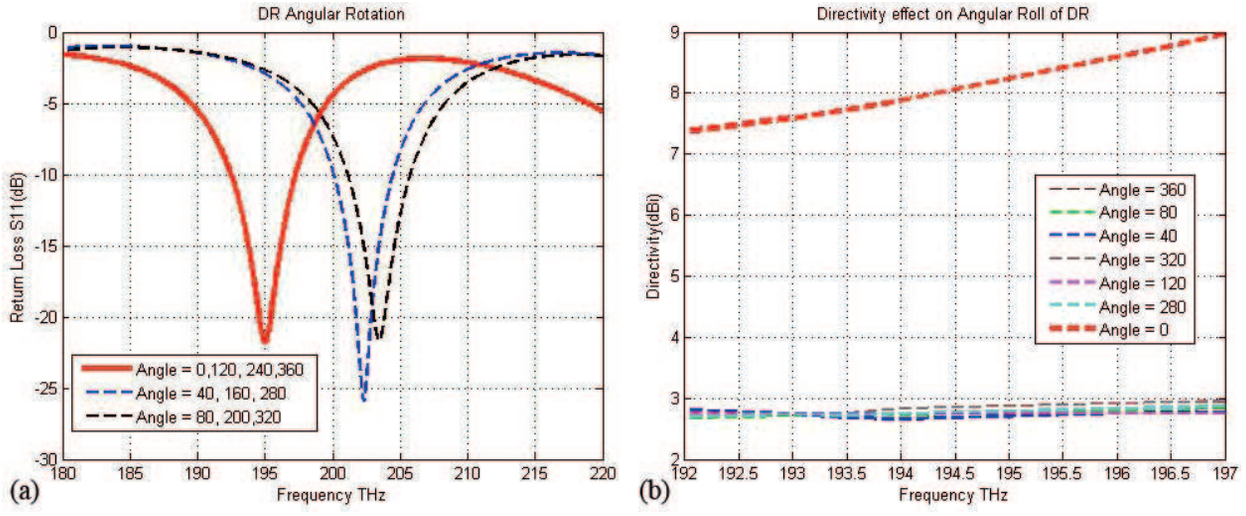

Figure 8. Optimized parameters: (a) effect of angular rotation of resonant frequency; (b) effect of angular rotation on directivity.

Parameters	Value (μm)
Feed length L_f	0.186
Feed width W_f	0.067
Ground length L_g	2.5
Ground width W_g	2
Height of triangular DR h	0.2
Area of triangular side a	1
Rotation angle θ	0^0

Table 1. Optimised parameters of ETDRN.

After extensive optimisation of stated parameters above and analysing the results achieved from these optimisations, the best geometric parameters that achieve an impedance bandwidth of 2.5% (192.3–197.3 THz) and a directivity of 8.6 dB are listed in **Table 1**. It is also observed that the simple ETDRNA structure can act as a tunable resonator when rotated around its axis resulting in usage of applications that work in the wavelengths in the range of (1463–1500 nm). The proposed design, if facility exists, can be fabricated via the known techniques involved in nanofabrication technology, that is, e-beam lithography, photolithography and chemical vapour deposition. In our case, the fabrication will follow a bottom-up approach where the SiO_2 substrate will have silver deposited on its surface.

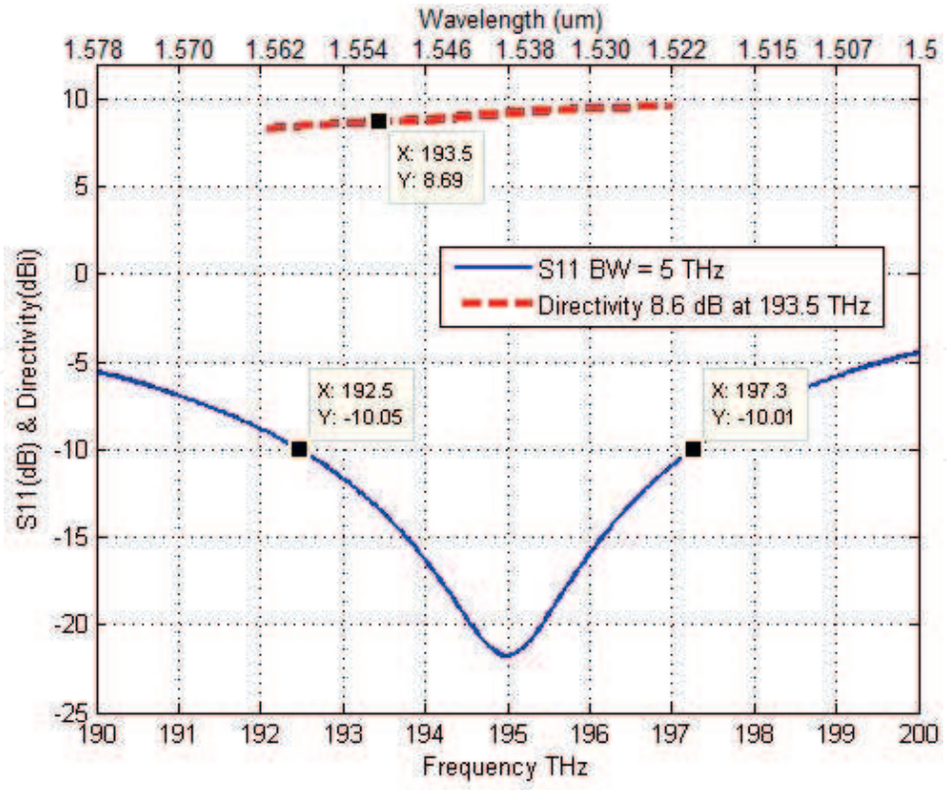

Figure 9. Simulated return loss and directivity of ETDRNA.

3.3. Results and discussion

In this section, we present the simulation results. **Figure 9** shows the return loss (S_{11}) and directivity of the proposed ETDRNA. The three-dimensional (3D) radiation patterns of the nanoantenna at 192, 193.5 and 197 THz are shown in **Figure 10(a–c)**. The maximum dip of −22 dB is achieved from the resonance of the nanoantenna at the central frequency of 1936.5 THz. The nanoantenna covers some part of the S-band while most part is covered for the C-band optical communication window. 3D radiation patterns provide the proof of the ETDRNA radiating in end-fire pattern. At present, the nanofabrication technology is limited and the proposed design is a theoretical one, yet we believe that our contribution in the fast-growing field of nantennas, with the proposed ETDRNA design, will prove itself to be a promising candidate for next-generation energy harvesting and green sustainable solution applications based on nanotechnology designs.

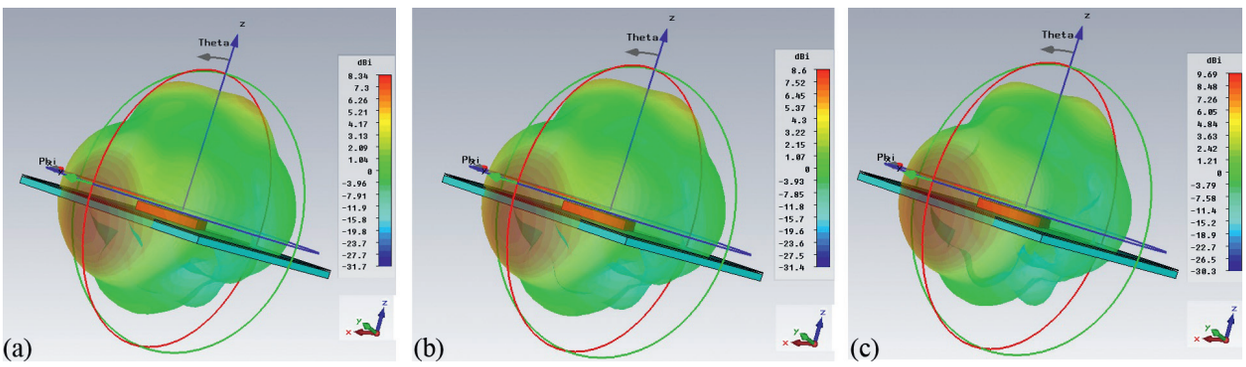

Figure 10. 3D end-fire radiation pattern at: (a) 192 THz, (b) 193.5 THz, (c) 197 THz.

4. Hexagonal dielectric resonator nantenna

In this section, we present another nantenna design based on dielectric resonator material. The shape of this DR is in hexagonal form with the material chosen as silicon (Si). The proposed design works as a loading element. The structure is again in multilayer form having (SiO_2) sandwiched between two silver (Ag) sheets. The radiating element is an equal-sided hexagonal-shaped (Si) dielectric loaded material. The whole nantenna structure is excited via a nanostrip transmission line made from a noble silver metal (Ag) whose conductive properties are calculated using the Drude model. The antenna achieves an impedance bandwidth of 3.7% (190.9–198.1 THz) with a directivity of 8.6 dBi at the frequency of interest. The obtained results make the proposed nantenna a possible solution for future nanophotonics and nanoscale communication devices.

4.1. Antenna geometry

In this section, we present another dielectric resonator (DR) design that takes the shape of a hexagon. The proposed nanoantenna works utilised the loading properties of ceramic dielectric

silicon and is termed as hexagonal dielectric loaded nantenna (HDLN). It is also designed to operate at the central frequency of 193.5 THz which corresponds to a wavelength of 1550 nm. The cross-sectional and front view of the proposed HDLN is in **Figure 11(a)** and **(b)**. The design is based on a multilayer structure with (SiO_2) substrate sandwiched between two noble metals each made from silver (Ag). The properties of substrate are: thickness of h_1 = 0.150 μm, ε_r = 2.1 and loss tangent *tan* δ = 0.003 at f = 100 THz [39]. The ground layer, made from silver, below the substrate has partial form with properties as thickness of t = 0.010 μm and dimensions $L_g \times W_g$ = 1.95 × 2 μm. The feeding line is a nano silver strip on top of the substrate with parameters: thickness h_2 = 0.025 μm, W_f = 0.067 μm and L_f = 0.186 μm. The substrate dimensions are taken as $W_s \times L_s$ = 5 × 5 μm^2. The hexagonal dielectric is made of (Si), with ε_r = 11.9 and estimated loss tangent, *tan* δ = 0.0025. To achieve a further increase in the bandwidth with minimum resonance losses, a small substrate with thickness h_3 = 0.015 μm made from (SiO_2) has been introduced between the hexagon and the nanostrip. The dimensions of hexagonal dielectric are calculated from Eq. (8) [43] by inscribing the hexagon inside a circle and equating the areas of both designs, thus giving an optimised equal side lengths of hexagon as s = 1 μm and thickness ($\lambda_g/4 < h < \lambda_g/2$) h = 0.377μm;

$$\pi a_e^2 = \frac{3\sqrt{3}}{2} s^2 \tag{8}$$

where a_e = area of the circle and s = side of the hexagon. Since at optical frequencies, metals appear with a negative permittivity; therefore, complex permittivity 'ε_{Ag}' of silver (Ag) calculated from Eq. (9) was explained by the Drude model [39]:

$$\varepsilon_{Ag} = \varepsilon_o \left\{ \varepsilon_\infty - \frac{f_{p^2}}{[f(f + i\gamma)]} \right\} = -128 + j3.28 \tag{9}$$

where ε_o = 8.85 × 10^{-12} [F/m], ε_∞ = 5, plasmonic frequency f_p = 2175 THz, f = central frequency and collision frequency γ = 4.35 THz. **Figure 11(b)** illustrates the antenna operating in the transmitting (Tx) mode by means of propagation vector orientation (k). The magnetic and electric field distributions of the hexagonal dielectric and nanostrip waveguide, along with the wave propagation in the y-axis, are also shown. Optical nantennas can be excited with a few known techniques ; (1) coupling of light using the so called nanotapers [46–47] since nano antennas cannot handle much power because of their small footprints, this makes them ideal candidates for being excited by micro lasers such as micro disks and photonic crystal lasers and (2) by reducing the reflection induced power loss by using slot dielectric waveguides [48].

4.2. Design simulation and optimisation

In this section, we make use of the optimisation techniques available to us from the simulator. We investigate the performance of each parameter involved in the design geometry of the proposed nanoantenna as shown in **Figure 11**. In order to study the impact on the antenna performance in terms of bandwidth, the following parameters have been studied and analysed.

http://dx.doi.org/10.5772/intechopen.69064

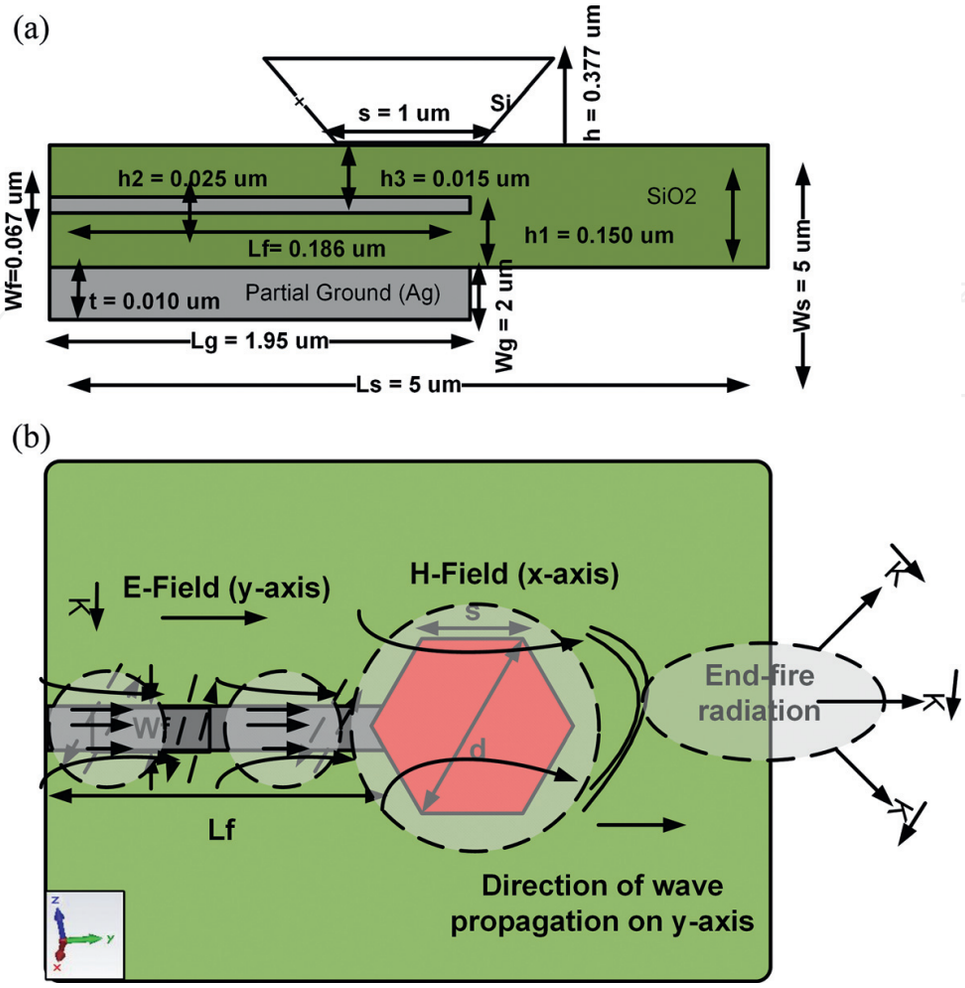

Figure 11. Geometry of hexagonal dielectric loaded nantenna (HDLN): (a) cross-sectional view; (b) front view with field vectors.

a. Nanostrip feed: Properties of conducting materials change when working at optical frequencies. The silver nanostrip line used to feed the nanoantenna was analysed in terms of Drude model. The nanostrip acts like a coupling resonator that excites the hexagonal dielectric, placed on an upper SiO_2 substrate with height h_3. Traditionally at RF frequencies, the length of the transmission lines is characterised to the wavelengths (λ) of incoming and outgoing radiations. However, working at the optical frequencies most of the incident light is transparent through the metals. This gives rise to plasmonic-free electrons, thus the feed line is analysed considering shorter effective wavelength (λ_{eff}), which depends on the material properties [44], refractive indexes and Eqs. (6) and (7). In our simulations, the optimised dimensions of the feed line produced values of length L_f to be 0.27 μm. The length L_f of the nanostrip stub was optimised from 0.1 to 0.27 μm with the best optimised value producing required resonance at 193.5 THz was at $L_f = 0.186$ μm as shown in **Figure 12(a)**. Similarly, the width 'W_f' of the nanostrip was also examined and optimisation was done from 0.02 to 0.28 μm. **Figure 12(b)** shows the best optimised value achieved at resonance of −22 dB with $W_f = 0.067$ μm.

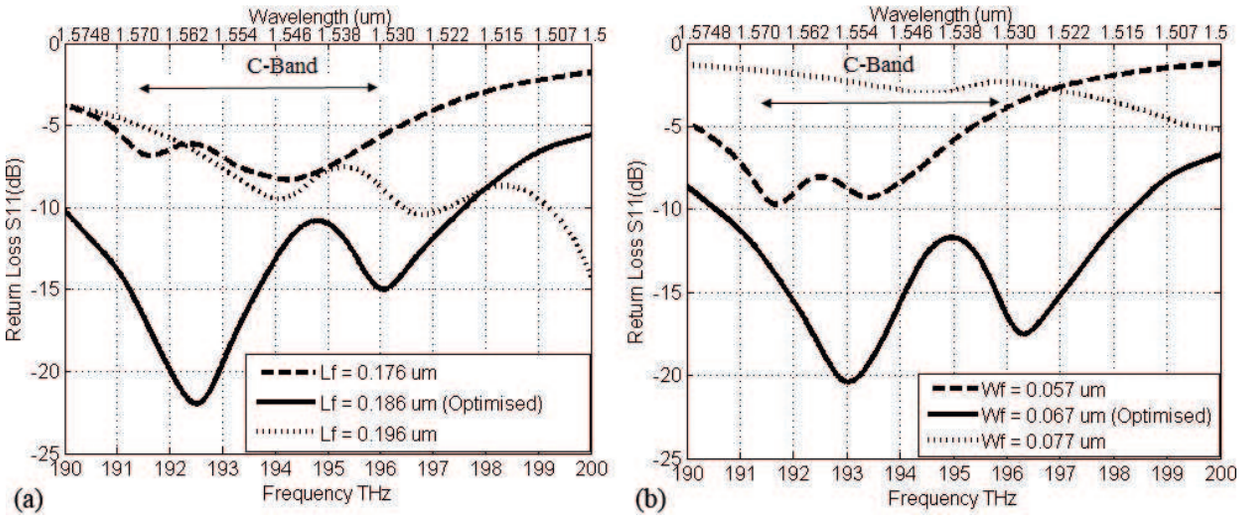

Figure 12. Optimized parameters: (a) length of feed line; (b) width of feed line.

b. **Partial ground plane:** The effect of the ground plane was studied and its optimisation gave dimewnsions of $L_g \times W_g = 1.95\ \mu m \times 2\ \mu m$. **Figure 13(a)** and **(b)** shows the effects of varying the partial ground plane in terms of its length and width. The optimised results produce a wide impedance bandwidth of 3.7% (190.9–198.1 THz) at a centre frequency of 193.5 THz, covering all of the standard optical transmission widow (C-band).

c. **Height of hexagonal DR:** The wide impedance bandwidth achieved is also affected by the height of the hexagonal DR. The height h of the DR was optimised within the range ($\lambda_g/4 < h < \lambda_g/2$) [3]. **Figure 14** shows the best optimised value of $h = 0.37\ \mu m$ having a resonance at −23 dB.

4.3. Results and discussion

To compare the properties and results of our proposed HDLN nanoantenna, we first simulated a hexagonal dielectric resonator antenna at the lower frequency band [41]. Observations were

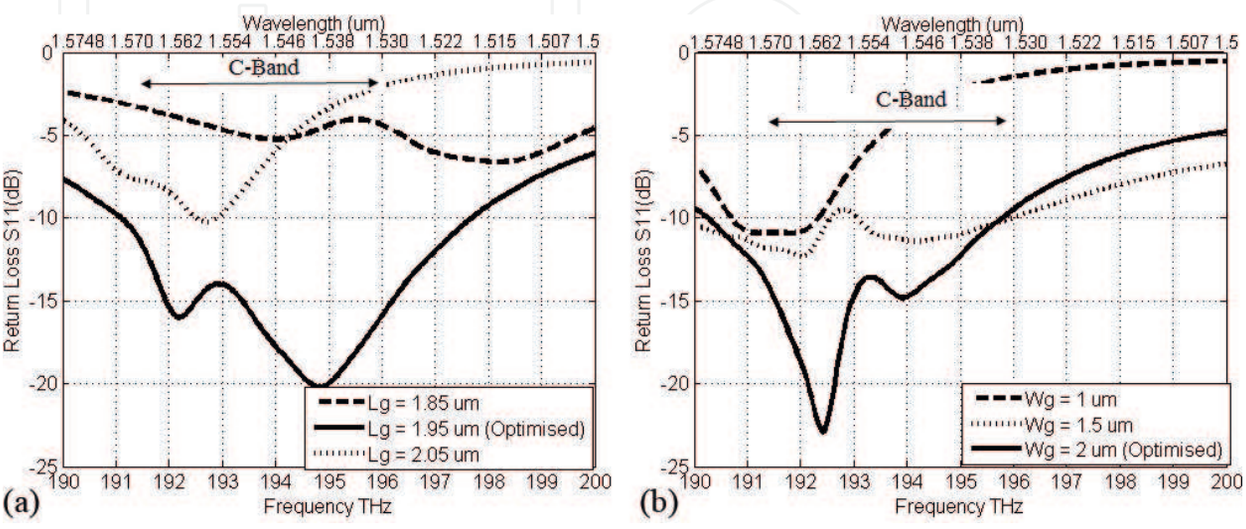

Figure 13. Optimized parameters: (a) length of ground plane; (b) width of ground plane.

http://dx.doi.org/10.5772/intechopen.69064

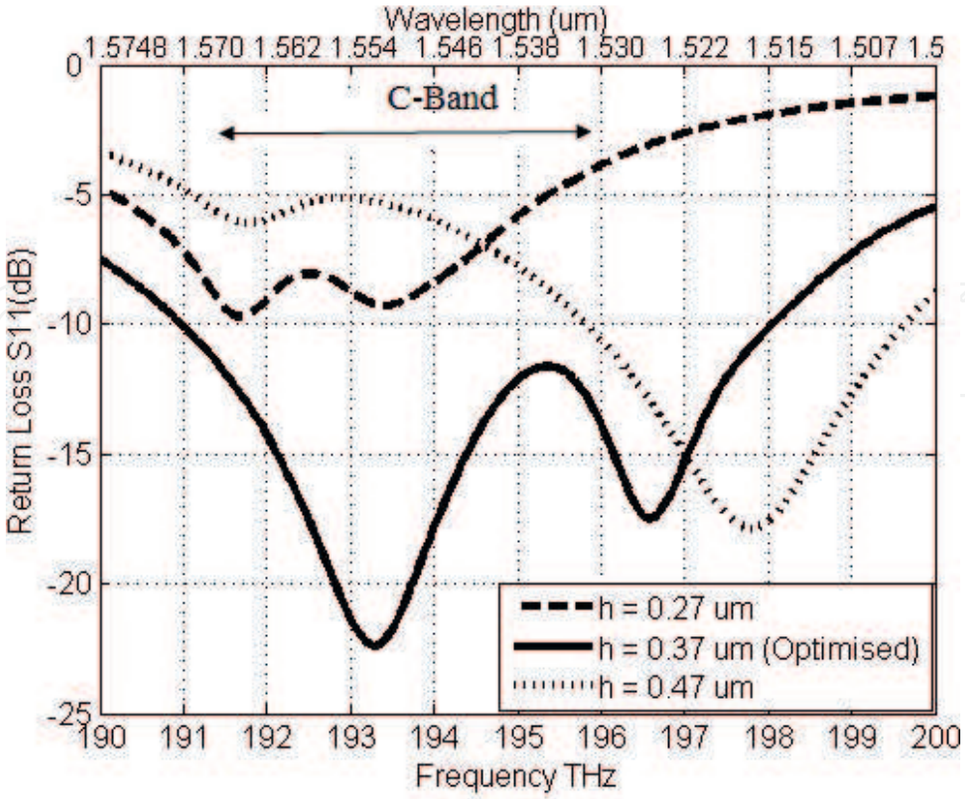

Figure 14. Optimised parameters: height of hexagonal DR.

made in terms of plane-wave propagation in the transmission lines to the radiating structures of the two antennas with results shown in **Figure 15(a)** and **(b)**, respectively. From **Figure 15 (a)**, it can be observed that the E-field propagation or the power propagation in the transmission line is following the fringing effects in order to radiate the hexagonal structure operating in the microwave domain. Whereas the proposed nantenna structure depicted in **Figure 15(b)** shows the E-field propagation in the nanotransmission line follows a travelling wave effect. It is also observed that the hexagonal DR elements for both the cases exhibit different properties. At the microwave domain, the hexagonal DR as shown in **Figure 15(a)** works as a resonator,

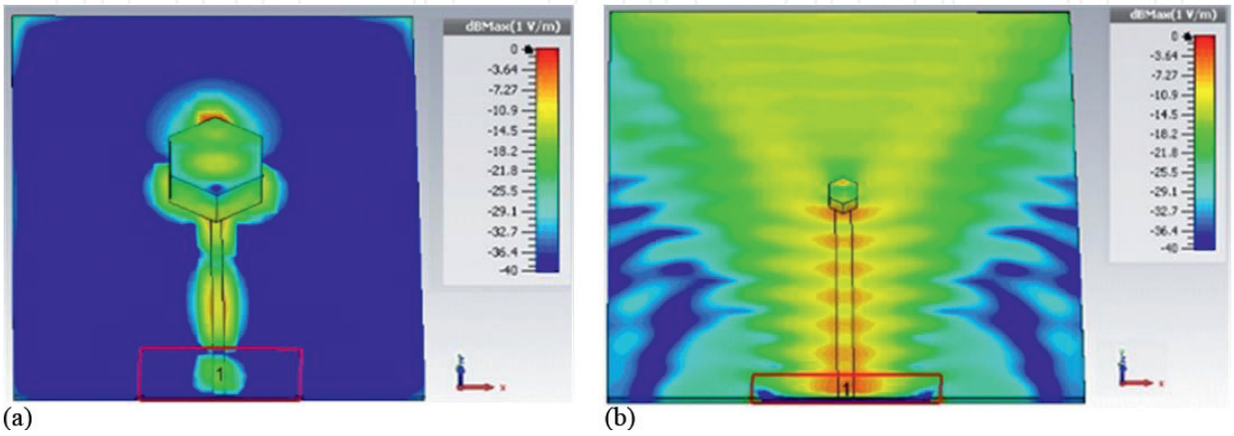

Figure 15. E-field propagation: (a) fringing effects at lower frequency; (b) travelling wave effect at THz spectrum.

whereas the DR at the nanoscale structure shown in **Figure 15(b)** exhibits loading properties which benefit the nantenna to operate as a lens and thus achieve more directivity.

The return loss (S_{11}) and directivity of the proposed HDLN with respective wavelength and directivity axis is shown in **Figure 16**. After extensive optimisation, the nantenna achieves an impedance bandwidth of 3.7% (190.9–198.1 THz) with a directivity of 8.6 dBi, making it useful for nanoscale fabrication due to its robustness against fabrication tolerances.

Typically, the modes of hexagonal DR [49] are derived from the cylindrical dielectric resonator, which has three distinct types: TE (TE to z), TM (TM to z) and hybrid modes. The TE and TM modes are asymmetrical and have no azimuthal variation. On the other hand, fields produced by hybrid modes are azimuthally dependent. Hybrid mode is further divided into two sub-groups of HE and EH. The modes generated by the hexagonal dielectric nantenna are represented in terms of magnitude of electric field distribution on its surface as shown in **Figure 17**, at the centre frequency of 193.5 THz. The mode analysis was done via EM simulator CST MWS.

From the infinite modes available [50], in our simulation as shown in **Figure 17**, we observed the nano hexagonal dielectric antenna producing $HE_{20\delta}$ mode between the achieved wide impedance band. The subscript in the modes represents the variation of fields along azimuthal, radial and *z*-direction of the cylindrical axis. It is observed from the figure that the magnitude of electric field variation is produced on the azimuthal direction with no variation in the radial direction, thus giving a mode excited at $HE_{20\delta.}$ Also, the intensity is highest at the azimuthal

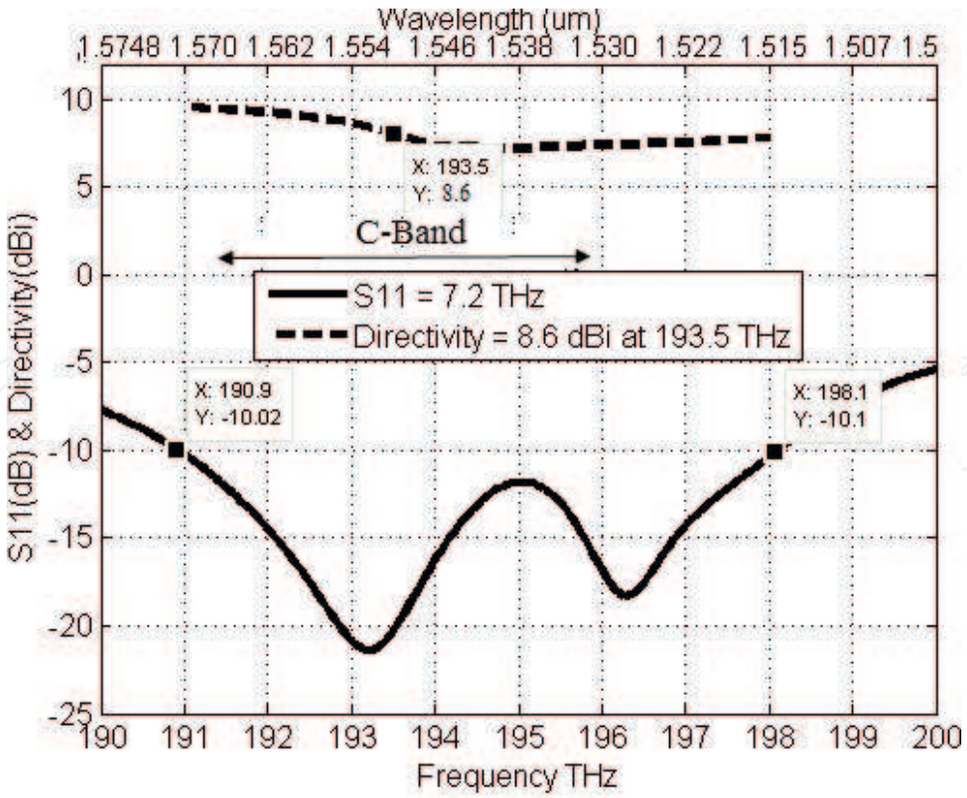

Figure 16. Simulated return loss and directivity of proposed HDLN.

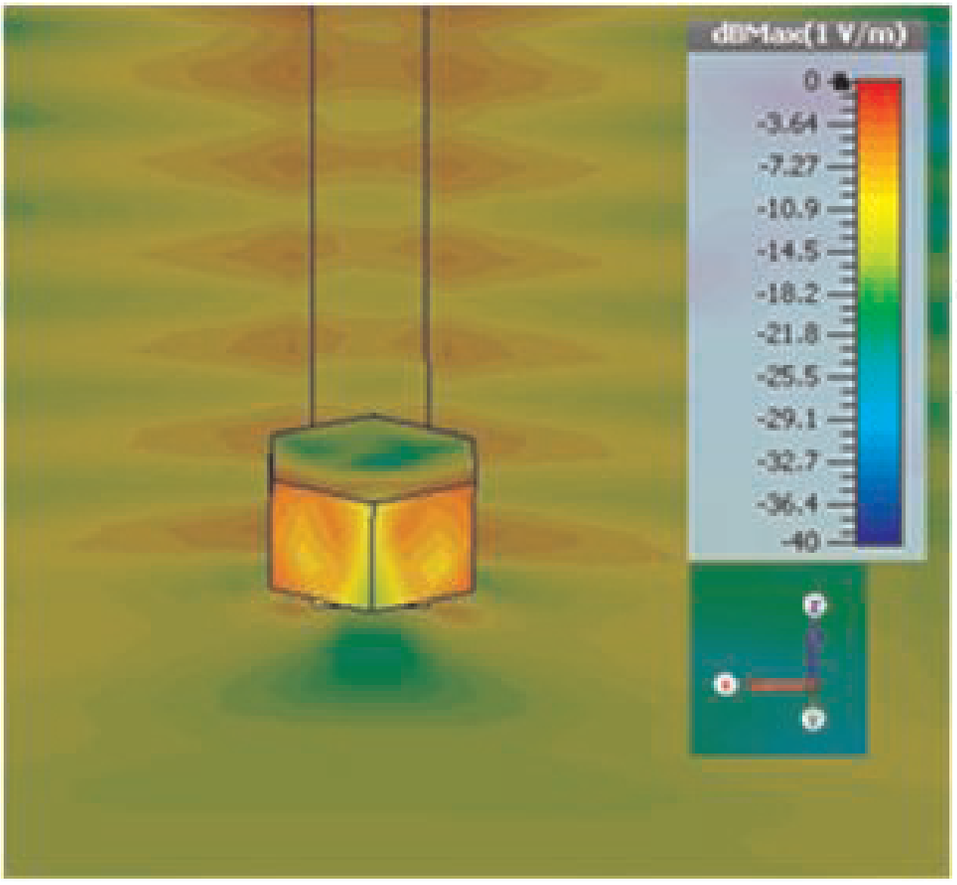

Figure 17. E-field distribution as shown via the magnitude at 193.5 THz with $HE_{20\delta}$ mode.

plane resulting in a radiation pattern towards the end-fire direction. The 3D radiation patterns of the nanoantenna at 191, 193.5 and 198 THz are shown in **Figure 18(a–c)**. The directivity of the antenna at the centre frequency is 8.6 dBi.

Keeping in mind the state-of-the-art nantenna designs and limited availability of nanofabrication equipment and facilities worldwide, we believe our proposed theoretical HDLN design will prove itself to be a promising communication device for applications based on nanotechnology.

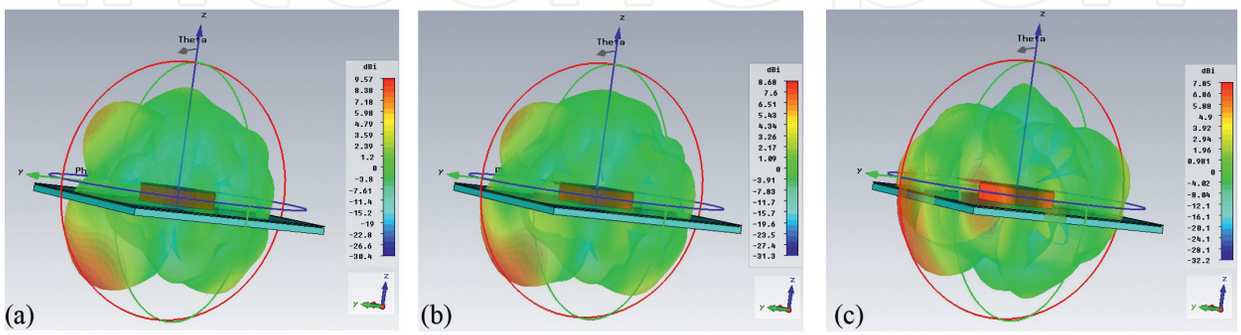

Figure 18. 3D radiation pattern: (a) 191 THz, (b) 193.5 THz and (c) 198 THz.

5. Array synthesis

In this section, we present the array synthesis done on one of the two proposed nantenna designs based on DR element. The ETDRNA was opted for array optimisation. The ETDRNA was fed via a 1 × 2 corporate feed network working at optical C-band (1.55 μm). Numerical results prove that the proposed nantenna exhibits a directivity of 9.57 dB with an impedance bandwidth of 2.58% (189–194 THz) covering the standard optical C-band transmission window. Furthermore, by selecting the appropriate orientation of the triangular dielectric resonators, the proposed nantenna structure can be tuned to operate at the higher or lower optical bands offering a threshold value of directivity and bandwidth Δf. By tuning the nantenna, they achieve an increase in bandwidth of 4.96% (185.1–194.7 THz) and directivity also improves to 9.7 dB. The wideband and directive properties make the proposed nantenna attractive for a wide range of applications including broadband nanophotonics, optical sensing, optical imaging and energy-harvesting applications.

5.1. Antenna array geometry

An array of 1 × 2 configuration for the ETDRNA is presented. The front and side view is shown in **Figure 19**. The geometry of the proposed nanoantenna utilised the same parameters as the proposed ETRDN in Section 3. The gap between the elements to counter mutual

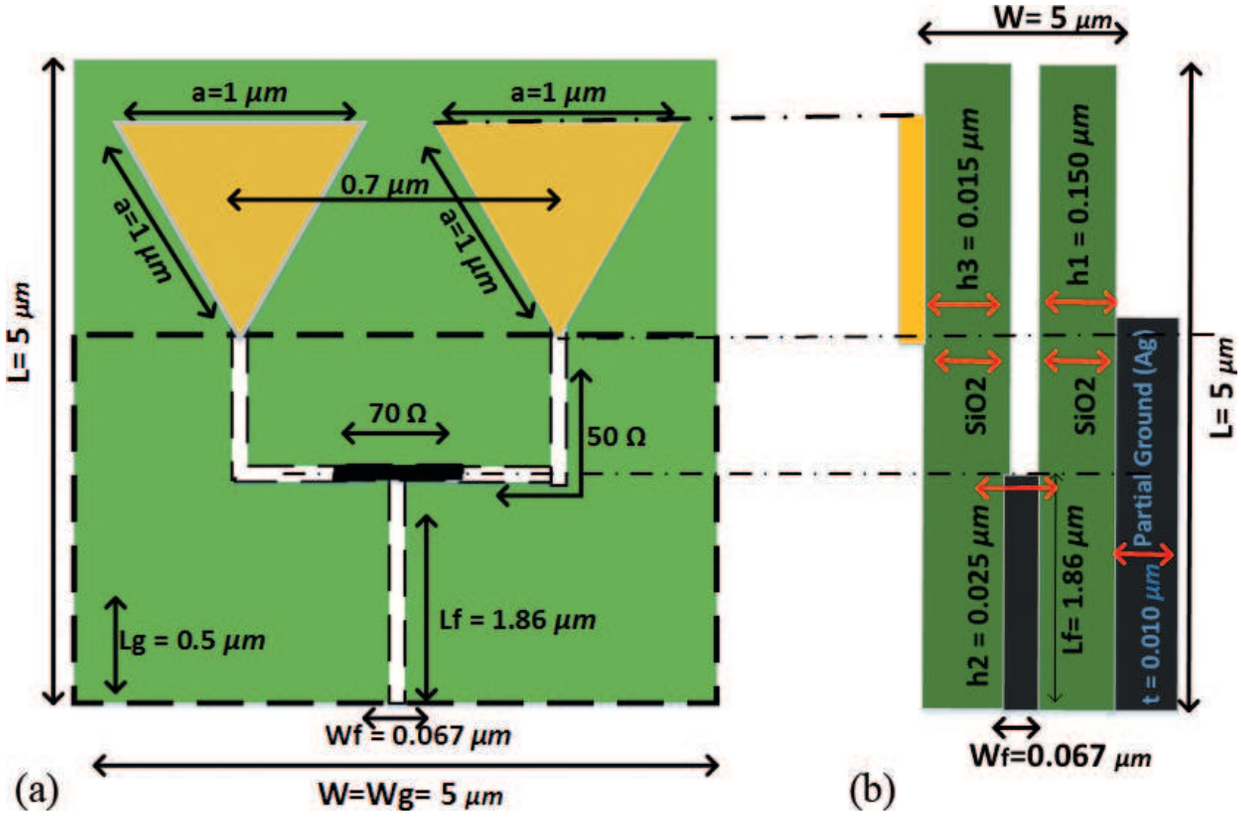

Figure 19. Geometry of proposed 1 × 2 array: (a) front view; (b) side view.

coupling is around (λ_{eff}/2) at the central frequency of 193.5 THz. The dimensions of the single element equilateral triangle dielectric based on frequency dependence can be calculated from Eqs. (1) and (2) previously presented in Section 3.

In order to increase the directivity of the proposed nantenna, arrays with a corporate feed network has been utilised for best power transfer from the source to the radiating ETDRNA. **Figure 19(b)** shows the corporate feed network along with appropriate feed line (50 and 70 Ω) markings. The optimised width of the 70 Ω feed line is 0.045 μm, whereas the length is 0.76 μm. For the 50 Ω feed line, the width and length are W_f and L_f, respectively. The shaded region in black shows the partial ground and feed lines to be on the backside of the substrate. The optimum distance between the triangular plasmonic resonators achieve minimal mutual coupling at 0.7 μm centre to centre. The properties of the noble metals are explained as per Drude Model used throughout the sections for the proposed nantenna designs.

5.2. Results and discussion

In this section, we investigate the proposed nanoantenna arrays results in terms of two important features: (1) directivity improvement and (2) tunability. Directivity is very important because it measures the power density the antenna radiates in the direction of its strongest emission versus the power density radiated by an ideal isotropic radiator (which emits uniformly in all directions) radiating the same total power, and on the other hand tunability is an attractive feature as it makes antenna operational in various frequency bands simultaneously as well as resonating at its centre frequency. In fact, during our performance analysis, we learned the importance of the angle of rotation between the triangular structure and the feed line direction. In the following paragraph and the next section, we first address the performance study when this angle is zero and then investigate the importance of this when different angles are introduced.

The simulated return loss (S_{11}) and directivity of the proposed 1 × 2 nanoantenna array are presented in **Figure 20**. The proposed nantenna achieves an impedance bandwidth of 2.58% with $S_{11} < -10$ dB (189–194 THz) at a centre frequency of 193.5 THz (1550 nm) with a dip at −15 dB. The antenna covers all the portion of the standard C-band transmission window in optical domain and can be used for relevant optical applications in nanonetworks and high-speed optical data transfer. The 3D radiation plot of the nantenna resonating at 193.5 THz is shown in **Figure 21**. The directivity of the nantenna is 9.57 dBi, 0.97 dB improvement compared to the single element ETDRNA discussed in Section 3. CST MWS studio has been used to acquire the optimised results with verification done by another EM simulator HFSS. Examining the plot in **Figure 21** reveals the E-field component having main lobe direction at 45°, side lobe levels at −4.1 dB and beam width of 20.1°. Similarly, the H-field component in **Figure 21** has main lobe direction of 180°, side lobe levels of −1.5 dB and beam width of 127.2°. Although the nantenna achieved a directive nature, the losses associated with high side lobe levels are to be expected due to substrate selection and working at higher THz frequencies.

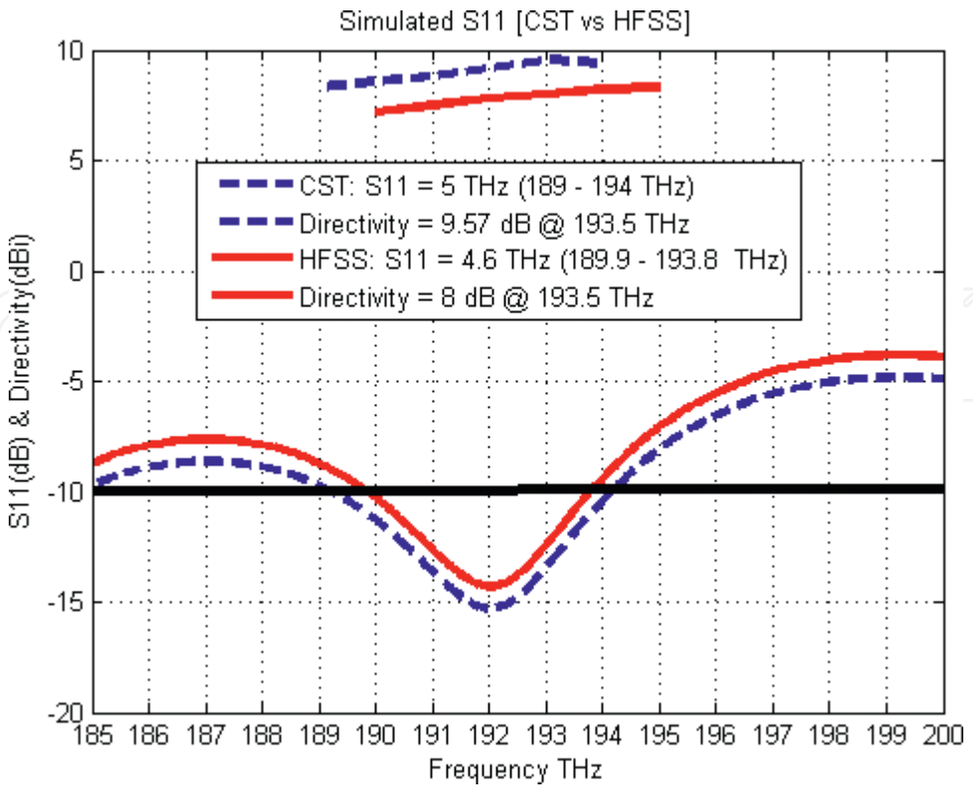

Figure 20. Return loss and directivity of 1×2 ETDRNA array.

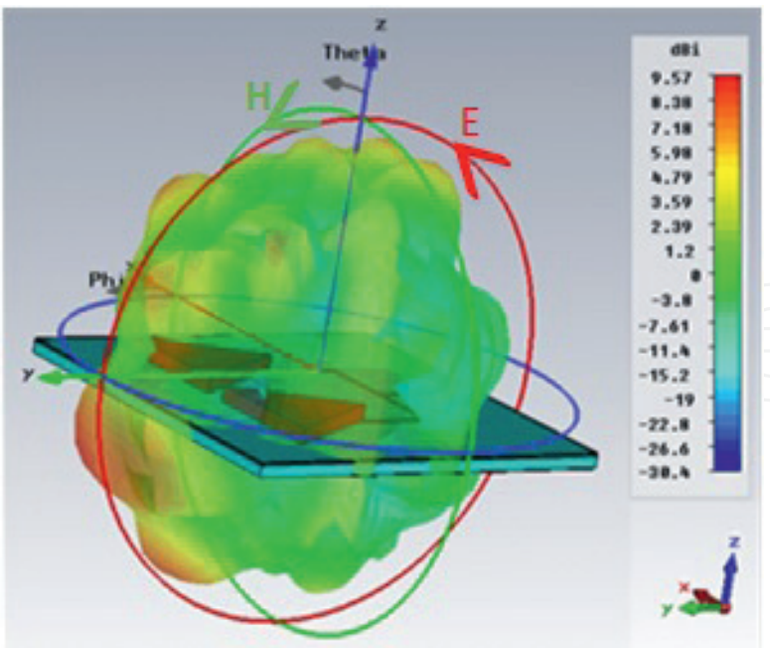

Figure 21. 3D radiation pattern at 193.5 THz.

5.3. Tunability of proposed 1 × 2 ETDRNA array

Achieving an antenna design for a specific frequency band (wide, notch or filter) with tunable (or changeable) centre frequency is an important challenge task. Our proposed nantenna array structure achieves this task and offers a large flexibility to the antenna in terms of operating frequency for a wide range of applications. Various parameters and design strategies such as loading slots, lumped components, switches, diodes and capacitors are introduced in order to achieve this feature. Although we have utilised a corporate feed network and the antenna geometry is based on nanoscale dimensions, which means more parametric study, but our simple and featured equilateral shape of the DR elements enable us to make natural yet simple tunability. **Figure 22** shows the rotation angles of the two equilateral triangular DR elements (T1 and T2). Since it is an equilateral triangle, the rotation angles were swept from (−180° to 180°) with a step size of 10°. The rotation angle is defined as counterclockwise movement from the bottom tip of the triangle. We apply three scenarios of rotations: (1) rotate T1 while T2 is fixed (**Figure 22a**), (2) fix T1 and rotate T2 (**Figure 22b**) and (3) simultaneously rotate T1 and T2 in the same counterclockwise direction (**Figure 22c**). In all the three scenarios, as shown in **Figure 22**, the simulation of rotation was done for the whole 360° but only five rotating angles

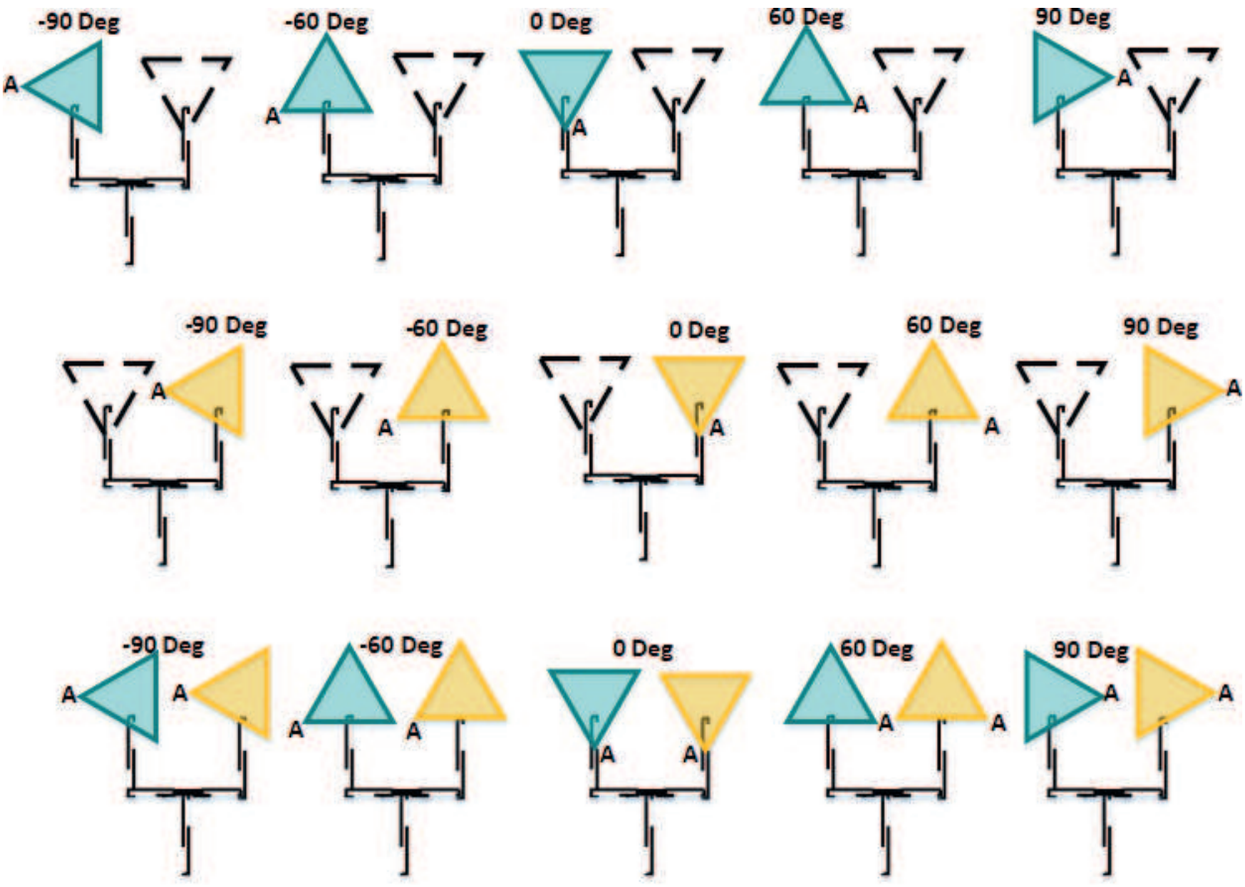

Figure 22. Rotation scenario of triangular DRs for spectral shifts: (a) rotate triangle T1 (left); (b) rotate triangle T2 (right) and (c) rotate both T1 and T2 simultaneously ± 90°.

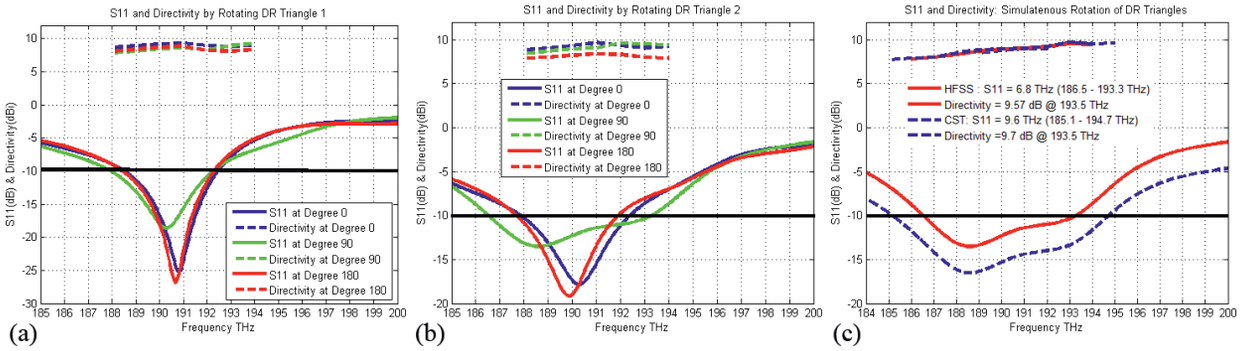

Figure 23. Return loss and directivity as per rotation: (a) T1 rotated; (b) T2 rotated and (c) both T1 and T2 simultaneously rotated.

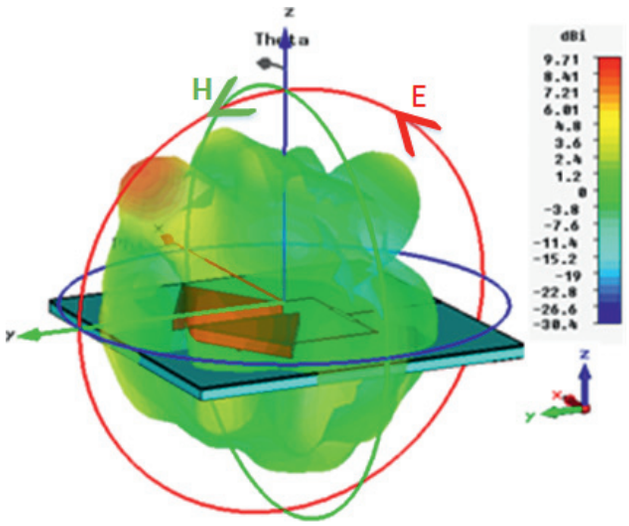

Figure 24. 3D radiation pattern of directivity at 193.5 THz after appropriate selection of DR triangular angles (−90° and 90°).

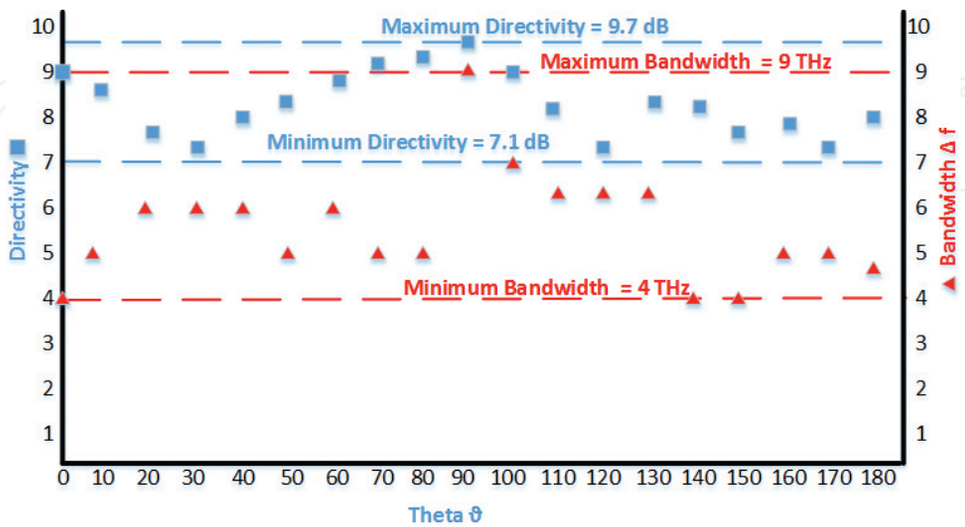

Figure 25. Effect of tunability on directivity and fractional bandwidth.

have been shown, that is, 0°, +60°, +90°, −60°, −90°, for purpose of simplicity. For our case of centre frequency at 193.5 THz, the best resonance with improved bandwidth of 4.96% (185.1–194.7 THz) and a directivity (9.7 dBi) is achieved when we opted to select the angles of T1 and T2 to be −90° and 90°, respectively. **Figure 23** displays the results in terms of s-parameters and directivity for rotation of triangles T1 and T2.

Figure 24, details of the E-field (yz-axis), shows main lobe at a direction of 45°, side lobe levels of −4.5 dB and beam width of 19°, whereas the H-field (xz-axis) has a main lobe direction of 115°, side lobe levels of −2.6 dB and beam width of 99.8° with a lot of losses in terms of high side lobe levels at a higher frequency. **Figure 25** shows the tunability effects of simulataneous rotation of triangular DRs in terms of the minimum and maximum values achieved for directivity and also the bandwidth difference Δf at −10 dB resonance in the frequency band (185–195 THz). The minimum directivity achieved is 7.15 dB and the maximum achieved is 9.71 dB when the triangles are tuned. Similary, the difference of bandwidth Δf ranges from a minimum to maximum of 4 to 9 THz, respectively.

6. Conclusion

In this chapter, we proposed two new optical nanoantenna designs working at centre frequency of 193.5 THz (1550 nm wavelength). We made use of dielectric resonators, which are ceramic based having very high dielectric permittivity, to assist the metallic designs mostly utilised in making plasmonic nanoantennas. Dielectric resonator (DR)-based antennas have made their mark and importance of antennas designed at the RF and MMW spectrum. Due to their unique feature of minimum surface loss and high radiation efficiency, they are considered nominal candidate to be used at higher spectrum bands, that is, THz.

Keeping with the offered characteristics of DR, we suggested two nanoantenna designs with triangular- and hexagonal-shaped DR materials. Both the designs are based on multilayer technology where the ground and transmission lines are made from noble metal silver. The properties of silver at optical domain are discussed and defined on the basis of Drude Model. The first design ETDRNA achieved an impedance bandwidth of 2.58% (192.3–197.3 THz), whereas the second nanoantenna design with hexagonal-shaped DR, HDLN, offered an impedance bandwidth of 3.7% (190.9–198.1 THz). Both the nanoantennas achieved high directivity of 8.6 dBi with end-fire radiation pattern. Array synthesis was also performed in order to compare and observe how much improvement is possible. The 1×2 ETDRNA achieved an improvement of 0.97 dB compared to the original directivity. Also the array antenna offers tunability in simple manner, compared to other methods discussed, making the proposed nanoantenna adaptable to many other optical frequency bands of interest for various optical communications.

Acknowledgements

This research work was supported by King Saud University, Deanship of Scientific Research and College of Engineering Center.

Author details

Waleed Tariq Sethi[1,2]*, Hamsakutty Vettikalladi[3], Habib Fathallah[2] and Mohamed Himdi[1]

*Address all correspondence to: wsethi@ksu.edu.sa

1 Institute of Electronics and Telecommunications of Rennes University (IETR), University of Rennes, France

2 KACST Technology Innovation Center in Radio Frequency and Photonics for the e-Society (RFTONICS), King Saud University, Riyadh, Saudi Arabia

3 Electrical Engineering Department, King Saud University, Riyadh, Saudi Arabia

References

[1] Cherry S. Edholm's law of bandwidth. IEEE Spectrum. 2004;**41**(7):58–60

[2] Li QC, Niu H, Papathanassiou AT, Wu G. 5G network capacity: Key elements and technologies. IEEE Vehicular Technology Magazine. 2014;**9**(1):71–78

[3] Stephan J, Brau M, Corre Y, Lostanlen Y. On the Effect of Realistic Traffic Demand Rise on LTE-A HetNet Performance. 2014 IEEE 80th Vehicular Technology Conference (VTC2014-Fall). Vancouver, BC; 2014. pp. 1–5

[4] Gregori M, Gómez-Vilardebó J, Matamoros J, Gündüz D. Wireless content caching for small cell and D2D networks. IEEE Journal on Selected Areas in Communications. 2016;**34**(5):1222–1234

[5] Mustafa IB, Uddin M, Nadeem T. Understanding The Intermittent Traffic Pattern Of HTTP Video Streaming Over Wireless Networks. 2016 14th International Symposium on Modeling and Optimization in Mobile, Ad Hoc, and Wireless Networks (WiOpt) (2016): n. pag. Web. 6 March 2017

[6] TU/e to develop 5G technology with European grant [Internet]. Available from: https://www.tue.nl/en/university/news-and-press/news/13-05-2016tueto-develop-5g-technology-with-european-grant/

[7] Valdes-Garcia A, Yong SK, Xia P. 60Ghz Technology For Gbps Wlan And Wpan. 1st ed. Hoboken, NJ: Wiley; 2013

[8] Chester E. 4.6Gbps Wi-Fi: How 60Ghz Wireless Works—And Should You Use It? Ars Technica. N.p., 2017. Web. 6 March 2017

[9] Researchers Demonstrate World's First 5G, 100 To 200 Meter Communication Link Up To 2 Gbps". Phys.org. N.p., 2017. Web. 6 March 2017

[10] Kürner T, Priebe S. Towards THz communications-status in research, standardization and regulation. Journal of Infrared, Millimeter, and Terahertz Waves. 2014;**35**(1):53–62

[11] Nagatsuma T, Ducournau G, Renaud CC. Advances in terahertz communications accelerated by photonics. Nature Photonics. 2016;**10**(6):371–379

[12] Petrov V, Pyattaev A, Moltchanov D, Koucheryavy Y. Terahertz band communications: Applications, research challenges, and standardization activities. Lisbon: 2016 8th International Congress on Ultra Modern Telecommunications and Control Systems and Workshops (ICUMT); 2016. pp. 183–190

[13] Lukasz L, Brzozowski M, Kraemer R. Data Link Layer Considerations for Future 100 Gbps Terahertz Band Transceivers. Wireless Communications and Mobile Computing. Vol. 2017. Article ID 3560521, 11 pages, 2017

[14] Yilmaz T, Akan OB. On the use of low terahertz band for 5G indoor mobile networks. Computers and Electrical Engineering. 2015;**48**:164–173

[15] Akyildiz IF, Jornet JM, Han C. Terahertz band: Next frontier for wireless communications. Physics Communications. 2014;**12**:16–32. DOI: 10.1016/j.phycom.2014.01.006 ()

[16] Obayya S, Areed NFF, Hameed MFO, Hussein M. Optical nano-antennas for energy harvesting. In: Innovative Materials and Systems for Energy Harvesting Applications. Hershey, PA, USA: IGI Global; 2015. p. 26

[17] Yang Y, Li Q, Qiu M. Broadband nanophotonic wireless links and networks using on-chip integrated plasmonic antennas. Scientific Reports. 2016;**6**:19490. DOI: 10.1038/srep19490

[18] Yousefi L, Foster AC. Waveguide-fed optical hybrid plasmonic patch nano-antenna. Optics Express. 2012;**20**(16):18326–18335

[19] Hong SG, et al. Bioinspired optical antennas: Gold plant viruses. Light: Science & Applications. 2015;**4**:267–272

[20] Horiuchi N. Optical antennas: Reconfigurable resonance. Nature Photonics. 2016;**10**(5): 2680–2685

[21] Jornet JM, Akyildiz AF. Channel modeling and capacity analysis for electromagnetic wireless nanonetworks in the terahertz band. IEEE Transactions on Wireless Communications. 2011;**10**(10):3211–3221

[22] Novotny L, van Hulst N. Antennas for light. Nature Photonics. 2011;**5**:83–90

[23] Palik ED. Handbook of Optical Constants of Solids. New York: Academic Press; 1998

[24] Johnson PB, Christy RW. Optical constants of the noble metals. Physical review B, APS Physics. 1972;**6**(12):5056–5070

[25] Petosa A, Ittipiboon A. Dielectric resonator antennas: A historical review and the current state of the art. IEEE Antennas and Propagation Magazine. 2010;**52**:91–116

[26] Luk KM, Leung KW, editors. Dielectric Resonator Antennas. Baldock, England: Research Studies Press; 2003

[27] Petosa A. Dielectric Resonator Antenna Handbook. Norwood, MA: Artech House; 2007

[28] Keyrouz and Caratelli D. Dielectric resonator antennas: Basic concepts, design guidelines, and recent developments at millimeter-wave frequencies. International Journal of Antennas and Propagation. 2016;**10**:0–20

[29] Belov PA, et al. Superdirective all-dielectric nanoantennas: Theory and experiment. IOP Conference Series: Materials Science and Engineering. 2014;**67**:012008–012013

[30] Devi I, et al. Modeling and design of all-dielectric cylindrical nanoantennas. Journal of Nanophotonics. 2016;**10**(4):046011–046011

[31] Andryieuski A, Malureanu R, Biagi G, Holmgaard T, Lavrinenko A. Compact dipole nanoantenna coupler to plasmonic slot waveguide. Optics Letters. 2012;**37**:1124–1126

[32] Suh JY, Huntington MD, Kim CH, Zhou W, Wasielewski WR, Odom TW. Extraordinary nonlinear absorption in 3d bowtie nanoantennas. Nano Letters. 2012;**12**:269–274

[33] Maksymov IS, Miroshnichenko AE, Kivshar YS. Actively tunable bistable optical yagi-uda nanoantenna. Optics Express. 2012;**20**:8929–8938

[34] Patel SK, Argyropoulos C. Plasmonic nanoantennas: Enhancing light-matter interactions at the nanoscale. EPJ Applied Metamaterials. 2015;**2**:03140–03174

[35] Giannini V, et al. Plasmonic nanoantennas: Fundamentals and their use in controlling the radiative properties of nanoemitters. Chemical Reviews. 2011;**111**(6): 3888–3912

[36] Wu CH, et al. Multimodal magneto-plasmonic nanoclusters for biomedical applications. Advanced Functional Materials. 2014;**24**(43):6862–6871

[37] Maksymov IS. Magneto-plasmonic nanoantennas: Basics and applications. Reviews in Physics. 2016;**1**:36–51

[38] Professor Nicholas Fang's Research Group @ MIT. Web.mit.edu. N.p., 2017. Web. 6 March 2017

[39] Johnson PB, Christy RW. Optical constants of the noble metals. Physical Review B. 1972;**6** (12):4370–4379

[40] Sinha R, Karabiyik M, Al-Amin C, Vabbina PK, Guney DO, Pala N. Tunable room temperature THz sources based on nonlinear mixing in a hybrid optical and THz micro-ring resonator. Scientific Reports. 2015;**5**:9422

[41] Lo HY, Leung KW, Luk KM, Yung EKN. Lowprofile equilateral-triangular dielectric resonator antenna of very high permittivity. Electronics Letters. 1999;**35**(25):2164–2166

[42] Kishk AA. A triangular dielectric resonator antenna excited by a coaxial probe. Microwave and Optical Technology Letters. 2001;**30**(5):340–341

[43] Balanis C. Antenna Theory: Analysis and Design. New York, NY,USA: John Wiley & Sons; 2005

[44] Olmon RL, Raschke MB. Antenna-load interactions at optical frequencies: Impedance matching to quantum systems. Nanotechnology. 2012;**23**(44):444001

[45] Neubrech F, et al. Resonances of individual lithographic gold nanowires in the infrared. Applied Physics Letters. 2008;**93**(16)163105

[46] Hattori HT, Li Z, Liu D, Rukhlenko ID, Premaratne M. Coupling of light from microdisk lasers into plasmonic nanoantennas. Optics Express. 2009;**17**(23):20878–20884

[47] Li Z, Hattori HT, Fu L, Tan HH, Jagadish C. Merging photonic wire lasers and nanoantennas. Journal of Lightwave Technology. 2011;**29**(18):2690–2697

[48] Hattori HT, Li Z, Liu D. Driving plasmonic nanoantennas with triangular lasers and slot waveguides. Applied Optics. 2011;**50**(16):2391–2400

[49] Hamsakutty V, Mathew KT. Hexagonal dielectric resonator antenna: A novel DR antenna for wireless communication [Ph.D. thesis]. Department of Electronics, Cochin University of Science and Technology, Dyuhti, India, 2007.

[50] Mongia RK, Bhartia P. Dielectric resonator antennas: A review and general design relations for resonant frequency and bandwidth. International Journal of Microwave and Millimeter-Wave Computer-Aided Engineering. 1994;**4**(3):230–247

IntechOpen